CT breast dose reduction with the use of breast positioning and organ-based tube current modulation

Wanyi Fu
Carl E. Ravin Advanced Imaging Laboratories, Department of Radiology, Department of Electrical and Computer Engineering, Duke University, Durham, North Carolina 27705, USA

Xiaoyu Tian
Carl E. Ravin Advanced Imaging Laboratories, Department of Radiology, Department of Biomedical Engineering, Duke University, Durham, North Carolina 27705, USA

Gregory M. Sturgeon and Greeshma Agasthya
Carl E. Ravin Advanced Imaging Laboratories, Department of Radiology, Duke University, Durham, North Carolina 27705, USA

William Paul Segars
Carl E. Ravin Advanced Imaging Laboratories, Department of Radiology, Department of Biomedical Engineering, Duke University, Durham, North Carolina 27705, USA

Mitchell M. Goodsitt and Ella A. Kazerooni
Department of Radiology, University of Michigan, Ann Arbor, Michigan 48109, USA

Ehsan Samei[a)]
Carl E. Ravin Advanced Imaging Laboratories, Department of Radiology, Medical Physics Graduate Program, Departments of Physics, Biomedical Engineering, and Electrical and Computer Engineering, Duke University, Durham, North Carolina 27705, USA

(Received 2 May 2016; revised 31 October 2016; accepted for publication 14 December 2016; published 13 February 2017)

Purpose: This study aimed to investigate the breast dose reduction potential of a breast-positioning (BP) technique for thoracic CT examinations with organ-based tube current modulation (OTCM).
Methods: This study included 13 female anthropomorphic computational phantoms (XCAT, age range: 27–65 y.o., weight range: 52–105.8 kg). Each phantom was modified to simulate three breast sizes in standard supine geometry. The modeled breasts were then morphed to emulate BP that constrained the majority of the breast tissue inside the 120° anterior tube current (mA) reduction zone. The OTCM mA value was modeled using a ray-tracing program, which reduced the mA to 20% in the anterior region with a corresponding increase to the posterior region. The organ doses were estimated by a validated Monte Carlo program for a typical clinical CT system (SOMATOM Definition Flash, Siemens Healthcare). The simulated organ doses and organ doses normalized by $CTDI_{vol}$ were used to compare three CT protocols: attenuation-based tube current modulation (ATCM), OTCM, and OTCM with BP ($OTCM_{BP}$).
Results: On average, compared to ATCM, OTCM reduced breast dose by 19.3 ± 4.5%, whereas $OTCM_{BP}$ reduced breast dose by 38.6 ± 8.1% (an additional 23.8 ± 9.4%). The dose saving of $OTCM_{BP}$ was more significant for larger breasts (on average 33, 38, and 44% reduction for 0.5, 1, and 2 kg breasts, respectively). Compared to ATCM, $OTCM_{BP}$ also reduced thymus and heart dose by 15.1 ± 7.4% and 15.9 ± 6.2% respectively.
Conclusions: In thoracic CT examinations, OTCM with a breast-positioning technique can markedly reduce unnecessary exposure to radiosensitive organs in anterior chest wall, specifically breast tissue. The breast dose reduction is more notable for women with larger breasts. © *2016 American Association of Physicists in Medicine* [https://doi.org/10.1002/mp.12076]

Key words: breast dose, Monte Carlo, Organ-based tube current modulation, organ dose, thoracic CT

1. INTRODUCTION

Computed tomography (CT) has significantly benefitted the clinical diagnosis of a wide spectrum of diseases. In the past decades, the use of CT has grown exponentially. In 2014, approximately 81.2 million CT examinations were performed in the United States.[1,2] The increased number of CT examinations has led to concerns about the associated population-based radiation dose.[3] Significant efforts have been made to minimize unnecessary radiation exposure and maximize patient benefits through the development of dose reduction techniques.[4] These techniques generally aim to reduce the unnecessary exposure to major radiosensitive organs while maintaining the required image quality level.[5,6]

Breasts are among the most radiosensitive organs for female patients.[7,8] In thoracic CT examinations, although

breasts are usually not diagnostically targeted, they receive a considerable amount of radiation dose.[9–12] In an effort to protect superficial radiosensitive organs such as breasts, some vendors have developed organ-based tube current modulation (OTCM) techniques.[13] In one implementation of OTCM, the tube current (mA) is reduced by 80% in the anterior region (± 60°) of the patient with a corresponding increase in the posterior region (X-CARE, Siemens Healthcare). It has been reported that, with OTCM, breast doses can be reduced by 30–50% with no detrimental effect on image quality.[5,6,14] However, a major challenge associated with the OTCM technique has been the extension of the breasts being outside the dose reduction zone.[15] A previous study has shown that, without any constraint, when the patient is supine, the breast tissue extends within an average angular zone of 155°; this is larger than the 120° dose reduction zone angle.[16] In effect, for most women, at least one breast partly resides in the increased dose zone, between ± 75° and ± 84°.[17] Another challenge with OTCM and associated breast dose is that the outer breast region contains a higher percentage of glandular tissue, making it more susceptible to cancer.[18] Majority of breast malignant tumors first develop in the upper outer quadrant of the breast.[19] As a result, the effectiveness of OTCM has been questioned, especially for women with larger breasts.[15]

The purpose of this study was to evaluate the dose reduction potential of a specially designed breast-positioning technique for OTCM examinations. The breast-positioning technique was modeled by constraining most of the breast tissue to within the dose reduction zone. The dose reduction potential of this technique was evaluated across a library of phantoms with various ages, weights, and breast sizes. The organ doses were computed from Monte Carlo simulations with three CT scan protocols: attenuation-based tube current modulation (ATCM), OTCM, and OTCM with breast positioning altered (referred to as $OTCM_{BP}$).

2. MATERIALS AND METHODS

2.A. Computational phantoms

This study included models of 13 female adult patients (age range: 27–65 y.o., weight range: 52–105.8 kg) who received a chest and abdominal-pelvis, or a chest-abdominal-pelvis CT examination at our institution. The patients represented anatomical variability among clinical population with a broad range of age and BMI distribution (Fig. 1).

The models have been developed from the CT images of the patients.[20] Initially, large organs within the scan volumes were segmented to generate phantom masks followed by 3D-triangulated polygon models using a marching cubes algorithm. The polygon structure was translated to 3D nonuniform rational B-spline surface (NURBS) (Rhinoceros, McNeel North America, Seattle, WA). The remaining organs and structures were generated by morphing a template's corresponding anatomies. The template was segmented from high-resolution visible human female full-body images.[21,22]

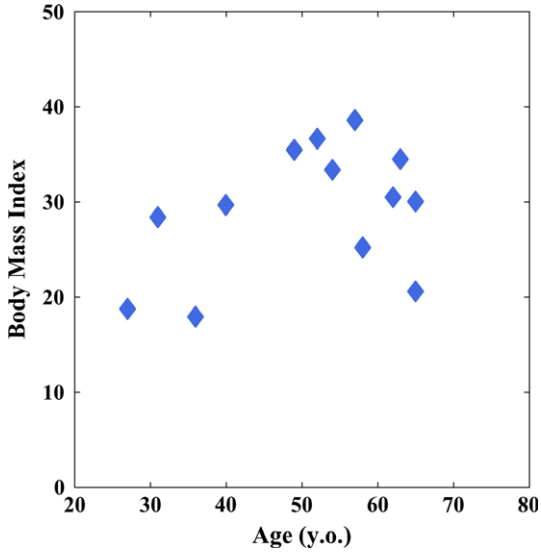

FIG. 1. BMI and age distribution of the computational phantoms. [Color figure can be viewed at wileyonlinelibrary.com]

The organ volume was rescaled to the organ volume and anthropometry data reported in ICRP 89.[23] The phantoms frontal views are shown in Fig. 2. Each phantom was voxelized at an isotropic resolution of 3.45 mm for input into a Monte Carlo simulation program. The resolution was chosen considering the anatomic details and simulation time.[24]

To investigate the effect of dose on glandular density, two compositions of breasts were simulated: (1) 50/50 breast (50% glandular tissue and 50% adipose tissue), as a representative case for younger women and (2) 20/80 breast (20% of glandular tissue and 80% adipose tissue), which was an approximation of mean glandular percentage in a wide population.[25–27]

2.B. Morphing the breasts

The phantom library was enhanced by modeling each phantom with three breast sizes (Fig. 3). To allow for the use of additional breast sizes, the torso surface of each phantom was first modeled as a smooth breast-free surface. The individual breasts were modeled as closed surfaces that were added to the breast-free surface. This modeling provided a library of 39 phantoms with the preserved breast-free surface and kept all other organs and structures constant.

Breast positioning (BP) was simulated on each phantom. The BP effectively modeled a support brassiere, which pressed breast tissue closer to the center of the torso to a greater extent than a normal brassiere. This ensured a majority of breast tissue within the ± 60° dose reduction zone. In order to facilitate the morphing, finite element models of the breasts were created.[28] A voxelized version of each breast (at isotropic resolution of 0.2 mm) was used to create hexahedral finite elements for each voxel. The elements adjacent to the midline of the torso or the imaginary breast-free torso surface were constrained to have zero displacement. This restricted the overall motion of the breast and provided a consistent

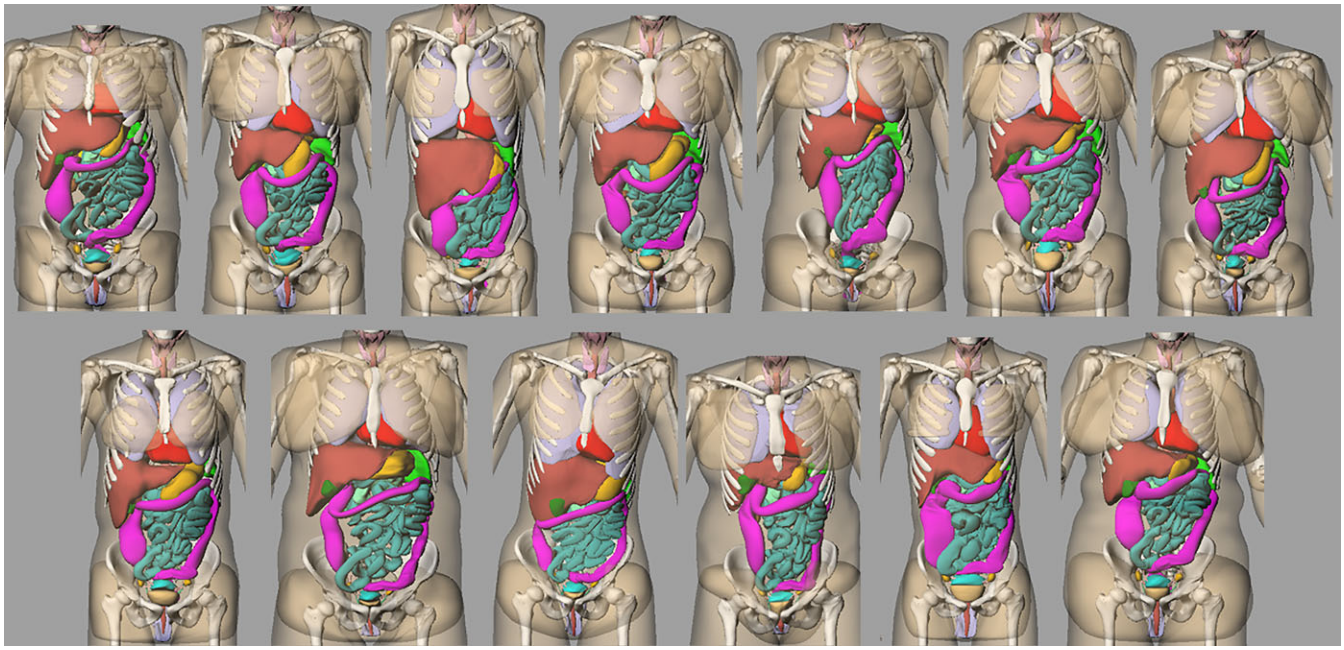

FIG. 2. 3D frontal view of the phantoms. [Color figure can be viewed at wileyonlinelibrary.com]

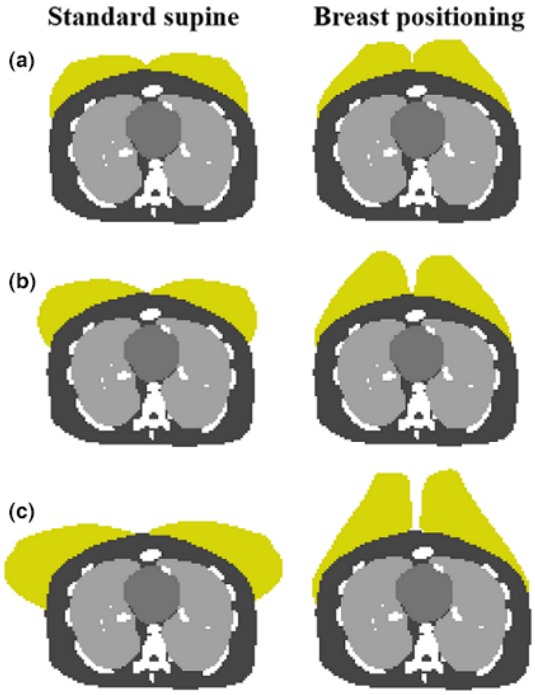

FIG. 3. Transverse slice of a modified voxelized XCAT phantom. Three breast sizes are shown: (a) small, (b) medium (c) large with breasts in standard supine position (left column) and the corresponding slice with breast-positioning technique (right column). The breast tissue is highlighted with light color. [Color figure can be viewed at wileyonlinelibrary.com]

attachment to the remainder of the body during the deformation. The breasts were modeled as a uniform hyperelastic Neo-Hookean material with a moduli of elasticity (E_adipose 1 kPa), which has been previously used for breast FE simulations,[29–31] and a nearly incompressible Poisson's ratio of 0.49. The deformation due to the BP support was approximated as a body force roughly tangential to the breast-free torso surface, where the magnitude of the body force was scaled to achieve the desired positioning. The resulting large deformation finite element model was solved using FEBio (University of Utah's Musculoskeletal Research Laboratories and Columbia's Musculoskeletal Biomechanics Laboratory).[32] The force was applied incrementally using 20 equal steps to account for the large deformations.

Deformation fields from the finite element analysis were applied to transform the polygon meshes and subsequently NURBS surfaces of each breast. Manual corrections were applied, when necessary, to further morph the breasts to ensure that the desired positioning was achieved and that the breast volume remained constant. Figure 3 shows an example phantom with three breast sizes before and after applying BP. The phantom library was further divided into three groups by breast size: small (447 ± 187 g), medium (1068 ± 222 g), and large-sized (1929 ± 432 g) groups. The percentage of breast volume within dose reduction zone in standard supine positioning and after applying BP is listed in Table I.

2.C. CT examination simulations

A previously validated Monte Carlo simulation program was used to simulate CT scans.[27,33] The package included PENOLOPE as a subprogram to track the energy loss of photons.[34,35]

A 64-section CT system (SOMATOM Definition Flash; Siemens Healthcare, Forchheim, Germany) was modeled.[36] The scan parameters were 120 kVp, pitch factor of 0.6, rotation time of 0.5 s, table speed of 2.304 cm/rot, 38.4 mm collimation, quality reference mAs of 150 mAs, and $CTDI_{vol}$ value denoted in Section 2.D. Clinical CT exams with ATCM

TABLE I. Mean of percentage of breast volume from all phantoms within ± 60° frontal zone with and without breast positioning (BP).

	Without BP (%)	With BP (%)	Change in Volume (%)
Small breasts	68.5 ± 11.1	93.9 ± 4.2	25.5 ± 12.1
Medium breasts	68.0 ± 17.0	93.7 ± 5.2	25.6 ± 14.3
Large breasts	57.2 ± 14.5	93.9 ± 3.3	36.6 ± 12.3
All Models	64.6 ± 15.2	93.8 ± 4.0	29.1 ± 14.1

were simulated for each standard supine phantom and OTCM simulated for all phantoms. The scan coverage was defined as 1 cm above lung apex to 1 cm below lung base.

The attenuation-based tube current modulation profile (mA_{ATCM}) simulated the virtual CAREDose4D, which takes into account attenuation of patient in both longitudinal (Z) and angular (XY) plane.[37] The XYZ attenuation through the phantom was simulated by a previously developed ray-tracing program.[24] At each projection angle θ, the 'fanbeam' function was used to measure the line integrals of attenuation coefficients alone each ray from the source to each detector bin (Matlab2010a; Mathworks, Natick, MA). The maximum line integrals of attenuation coefficients (ud) from all detector bins at θ was selected as the basis to generate tube current profile at θ. The tube current profile was modeled as

$$mA_{ATCM}(\theta) = mA_0 \times e^{\alpha \times ud(\theta)}, \quad (1)$$

where mA_0 and $mA_{ATCM}(\theta)$ are the fixed and attenuation-based modulated mA, respectively, $ud(\theta)$ is the maximum line integrals of attenuation coefficients calculated at θ, and α is the modulation strength.[38] A typical averaged modulation strength level ($\alpha = 0.5$) was used. Finally, at each rotation, the tube current was scaled to below the systems' maximum mA limit.

To generate the organ-based tube current profile (mA_{OTCM}) (X-CARE, Siemens Healthcare), the longitudinal (Z-plane) profile was reduced by 80% between ± 60° and the reduction was evenly divided and added to the remaining projections within one rotation. The angular (XY-plane) modulation was turned off.[13] The longitudinal-profile was modeled as

$$mA_Z(\theta) = 0.5 \times \left(mA_0 \times e^{\alpha \times ud(\theta_{AP})} + mA_0 \times e^{\alpha \times ud(\theta_{LAT})}\right), \quad (2)$$

where mA_0 and $mA_Z(\theta)$ are the fixed and longitudinal modulated mA respectively, $ud(\theta_{AP})$ and $ud(\theta_{LAT})$ are the attenuation in AP (anterior–posterior) and in LAT (lateral) direction along the Z-plane at gantry angle θ.[24] This approach emulated the CT system, in that the Z-profile was generated prior to the scan based on localization radiographs in LAT and AP directions.[24] The simulation further modeled gradual change in mA (slope as a function of rotation time, and upward- and downward-transition time) when switching between mA reduction and mA increase zone. Using 0.28 rot/s and 1 rot/s per Duan *et al.*,[13] the mA upward and downward times at 0.5 rot/s were estimated using linear approximation as 17% and 6% of rotation time respectively. The mA value was generated for models without and with BP separately, thus, referred to as mA_{OTCM} and $mA_{OTCM,BP}$, respectively. The mA_{ATCM}, mA_{OTCM}, and $mA_{OTCM,BP}$ of one example phantom is shown in Fig. 4.

2.D. Organ dose estimation

Organ doses were determined by tracking the energy deposited within each organ using flux for a particular $CTDI_{vol}$ value specific to each phantom as dictated by the average mA over the scan coverage of the applied TCM. The $CTDI_{vol}$ values for the phantoms scanned with OTCM and ATCM ranged from 4.7 to 16.2 mGy. With breast positioning, $CTDI_{vol}$ changed slightly by an average of 4 ± 5% reduction leading to a $CTDI_{vol}$ range of 4.5–17.1 mGy. The Size-Specific Dose Estimate (SSDE) was also calculated for each simulated scan using each phantom's chest water equivalent diameter[39] and the SSDE/$CTDI_{vol}$ conversion factors as defined by AAPM task group 204.[40] To report in detail, the $CTDI_{vol}$ and SSDE values for ATCM/OTCM and $OTCM_{BP}$ were fitted as an exponential function of chest water-equivalent diameters (Fig. 5). For $CTID_{vol}$, the fitting equations were $CTDI_{vol,ATCM/OTCM} = 0.56e^{0.09d}$ and $CTDI_{vol,OTCM_{BP}} = 0.49e^{0.1d}$ for ATCM/OTCM and $OTCM_{BP}$, respectively, where d represents chest water-equivalent diameter. For SSDE, the fitting equations were $SSDE_{ATCM/OTCM} = 2.12e^{0.06d}$ and $SSDE_{OTCM_{BP}} = 1.94e^{0.06d}$ for ATCM/OTCM and $OTCM_{BP}$, respectively. All fittings have $R^2 \geq 0.9$.

The organ doses were further normalized by $CTDI_{vol}$ to derive the $CTDI_{vol}$-to-organ dose conversion coefficients (h factors). As $CTDI_{vol}$ alone significantly influences dose, expanding the results in terms of h factors could be interpreted as a comparing technique where total flux (and thus image quality by implication) remains constant, so that the net effect of modulation alone on dose can be evaluated by comparing h_{ATCM} and h_{OTCM}. Similarly, the net effect of breast positioning alone can be evaluated by comparing h_{OTCM} and $h_{OTCM,BP}$. The breast dose was computed for both 50/50 and 20/80 homogeneous breasts.

The organ dose and h factors' percentage difference for breasts as well as other organs were calculated for OTCM, $OTCM_{BP}$, and ATCM, respectively. Organs were further grouped into anterior organs, medial or distributed organs, and posterior organs based on organ geometric center locations with respect to the isocenter of CT scanner.

Because breast positioning repositions more breast volume within the dose reduction zone for larger breasts (Table I), in order to assess the effect of breast mass on dose reduction potential, the breast dose value and h factors were further fitted to breast mass as

$$\hat{D}_{breast} = p_{D,1} m_{breast} + p_{D,2} \quad (3a)$$

$$\hat{h}_{breast} = p_{h,1} m_{breast} + p_{h,2}, \quad (3b)$$

where $\hat{D}_{breast}$ and $\hat{h}_{breast}$ denote the fitted breast dose and h factors for breasts, respectively, m_{breast} is the weight of both breasts in each phantom, and p_1 and p_2 are the linear fitting coefficients.

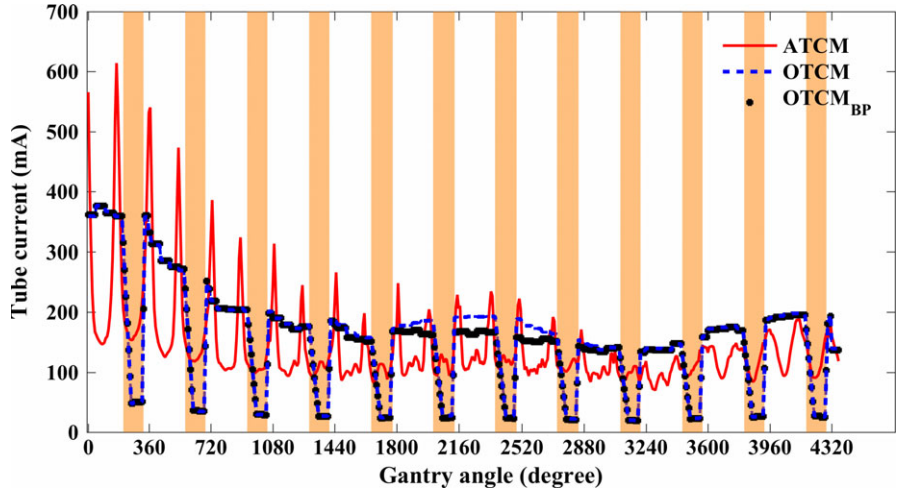

FIG. 4. An example of the tube current profile generated for attenuation-based tube current modulation (ATCM), organ-based tube current modulation (OTCM), and OTCM with breast positioning (OTCM$_{BP}$) for a phantom with breast mass of 1098 g (50/50 breast). The shaded regions correspond to the dose reduction zone. [Color figure can be viewed at wileyonlinelibrary.com]

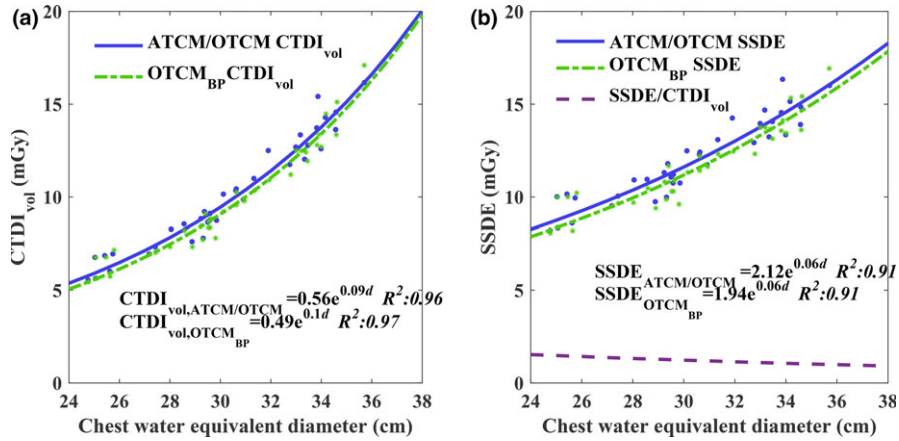

FIG. 5. (a) CTDI$_{vol}$ and (b) SSDE values for ATCM/OTCM and OTCM$_{BP}$ scans fitted to chest water-equivalent diameter. [Color figure can be viewed at wileyonlinelibrary.com]

To better estimate the overall organ dose reduction potential for OTCM and OTCM$_{BP}$, the average effective dose was calculated for ATCM, OTCM, and OTCM$_{BP}$. The effective dose was calculated as the sum of organ doses multiplied by tissue weighting factors defined by ICRP 103,[41] following the common practice of using effective dose as the scalar metric of radiation dose, even though, by definition, the effective dose can only be evaluated by reference phantoms. The doses for organs not explicitly modeled (salivary glands-, extrathoracic (ET) region-, oral mucosa-doses, lymphatic nodes-, and muscle-doses), were approximated by the doses to neighboring organs.[33]

In order to report the organ dose, an exponential regression model of h factors and chest diameter was calculated as

$$\hat{h} = e^{\alpha_h d + \beta_h}, \tag{4}$$

where $\hat{h}$ denotes the fitted h factors, α_h and β_h are the fitting coefficients, and d is the chest diameter. Thus, given the patient size and CTDI$_{vol}$ the organ dose can be rapidly predicted for this specific tube current modulation scheme and CT scanner.[36,37,42,43] Please note that this organ dose estimation technique is more accurate for organs within the scan coverage, where the majority of the dose is distributed.[38]

3. RESULTS

On average, compared to ATCM, OTCM reduced the 50/50 breast dose by 19.3 ± 4.5%. The average breast dose was further decreased by an additional 23.8 ± 9.4% to 38.6 ± 8.1% with OTCM$_{BP}$ compared to ATCM (Fig. 6). The corresponding percentage reduction in terms of h factors were 21.3 ± 7.3% (OTCM$_{BP}$ to OTCM) and 36.5 ± 6.9% (OTCM$_{BP}$ to ATCM), respectively. Table II shows the average breast dose and h factors for the 50/50 and 20/80 breasts simulated with ATCM, OTCM, and OTCM$_{BP}$. The difference in h factors between the two breast compositions was 8.8 ± 0.5%, and the two compositions exhibited very similar

trends in terms of impact of imaging method on dose. Figure 7 shows dose distribution plots of one phantom with small, medium, and large breasts undergoing ATCM, OTCM, and $OTCM_{BP}$ exams at a mid-transverse plane.

The breast dose saving of $OTCM_{BP}$ compared to ATCM was more significant for patients with larger breasts. For small (447 ± 187 g), medium (1068 ± 222 g), and large-sized (1929 ± 432 g) groups, $OTCM_{BP}$ and ATCM breast dose difference were −32.6 ± 7.0%, −38.3 ± 5.2%, and −44.8 ± 7.2%. The corresponding values in terms of *h* factors difference were −31.4 ± 6.5%, −36.8 ± 5.0%, and −41.3 ± 5.3%, respectively (Table III). Compared to OTCM alone, $OTCM_{BP}$ breast dose decreased by 18.7 ± 9.0%, 22.3 ± 7.1%, and 30.5 ± 8.2% for small-, medium-, and large-sized groups, respectively. The corresponding value in terms of *h* factors were 17.3 ± 7.8%, 20.4 ± 6.2%, and 26.2 ± 4.9%. The fitting coefficients of dose values vs. breast mass for the three protocols are given in Table IV (Fig. 8).

Figure 9 shows the organ dose differences between $OTCM_{BP}$ and ATCM, OTCM and ATCM, and $OTCM_{BP}$ and OTCM. Compared to ATCM, OTCM significantly reduced dose and *h* factors to general anterior organs (except larynx–pharynx) ($p<0.01$). Doses to several organs (large intestine, stomach, thymus, pancreases, and small intestine) decreased up to 10%. The doses to medial and posterior organ dose in OTCM compared to ATCM was increased by less than 10% ($p<0.01$). For distributed organs such as bone marrow and bone surface, which are located more toward posterior of the patient, organ doses were increased by ~10%. The skin dose remained relatively constant. When using BP compared to OTCM alone, all organ doses were decreased or not changed significantly. The corresponding *h* factors to anterior organs were decreased or not changed significantly and the *h* factors to medial and posterior organs were increased by less than 3% (except for spleen).

Table V shows the average effective dose results for 39 phantoms and different breast-sized groups. The results showed that the effective doses were similar for ATCM and OTCM with 4.8 ± 1.1 mSv and 4.6 ± 1.0 mSv, respectively. ATCM to OTCM effective dose reduction was ~6% for all breast-size groups. With BP, the average effective dose was reduced to 4.2 ± 1.0 mSv. Compared to ATCM, $OTCM_{BP}$ reduced effective dose by 11.2 ± 3.0%, 12.4 ± 3.6%, and 15.2 ± 6.0% for small-, medium-, and large-sized breast groups, respectively.

Figure 10 shows *h* factors fitted to patient chest diameter as an exponential function and Table VI shows the fitting coefficients. For organs within the scan coverage (lung, esophagus, heart, thymus, trachea-bronchi), the organ doses were more strongly correlated with chest diameters ($R^2 > 0.7$), except for breasts. For distributed organs, the correlations were moderate ($0.85 > R^2 > 0.6$). For organs on the periphery or outside of the scan coverage, the correlations were relatively small ($R^2 \leq 0.6$).

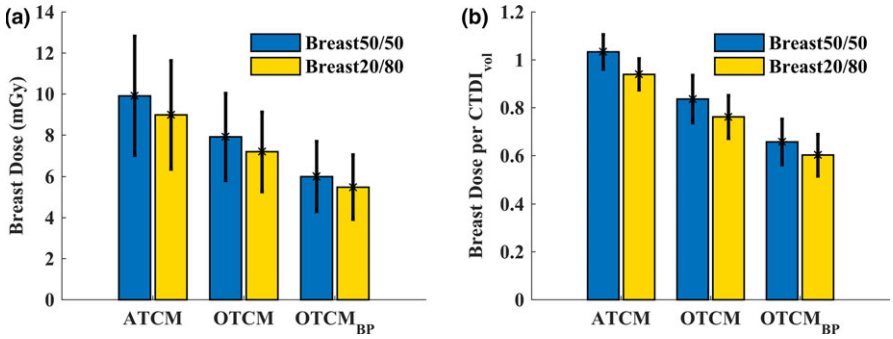

FIG. 6. (a) Breast dose and (b) average of $CTDI_{vol}$-normalized-breast breast dose coefficients simulated with ATCM, OTCM, and $OTCM_{BP}$ for all phantoms with 50/50 and 20/80 breasts. Error bars represent ± 1 standard deviation. [Color figure can be viewed at wileyonlinelibrary.com]

TABLE II. Average breast dose and the difference from ATCM, OTCM, and $OTCM_{BP}$.[a]

Breast dose						
Breast Composition	ATCM Dose (mGy)	OTCM Dose (mGy)	$OTCM_{BP}$ Dose (mGy)	$OTCM_{BP}$ to ATCM difference (%)	OTCM to ATCM difference (%)	$OTCM_{BP}$ to OTCM difference (%)
50/50	9.9 ± 2.9	7.9 ± 2.1	6.0 ± 1.7	−38.6 ± 8.1[b]	−19.3 ± 4.5[b]	−23.8 ± 9.4[b]
20/80	9.0 ± 2.6	7.2 ± 1.9	5.5 ± 1.6	−38.1 ± 8.1[b]	−19.2 ± 4.5[b]	−23.4 ± 9.3[b]
$CTDI_{vol}$-normalized breast dose coefficients						
Breast Composition	ATCM Dose per $CTDI_{vol}$	OTCM Dose per $CTDI_{vol}$	$OTCM_{BP}$ Dose per $CTDI_{vol}$	$OTCM_{BP}$ to ATCM difference (%)	OTCM to ATCM difference (%)	$OTCM_{BP}$ to OTCM difference (%)
50/50	1.0 ± 0.1	0.8 ± 0.1	0.7 ± 0.1	−36.5 ± 6.9[b]	−19.3 ± 4.5[b]	−21.3 ± 7.3[b]
20/80	0.9 ± 0.1	0.8 ± 0.1	0.6 ± 0.1	−36.0 ± 6.8[b]	−19.2 ± 4.5[b]	−20.8 ± 7.2[b]

[a]Negative means dose reduction.
[b]represents statistical significant.

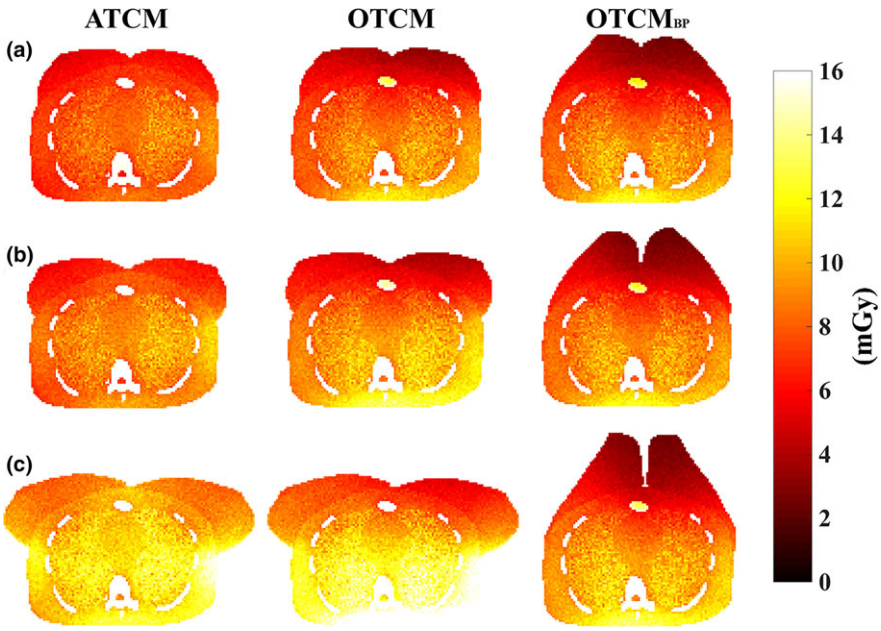

FIG. 7. Dose distribution plots of one example phantom with small (a), medium (b), and large (c) breasts. [Color figure can be viewed at wileyonlinelibrary.com]

TABLE III. Average breast dose coefficients and dose difference in different sized breast group.[a]

Breast dose						
Breast Size	ATCM Dose (mGy)	OTCM Dose (mGy)	$OTCM_{BP}$ Dose (mGy)	$OTCM_{BP}$ to ATCM difference (%)	OTCM to ATCM difference (%)	$OTCM_{BP}$ to OTCM difference (%)
Small	8.0 ± 2.5	6.5 ± 1.8	5.4 ± 1.9	−32.6 ± 7.0[b]	−16.9 ± 4.1[b]	−18.7 ± 9.0[b]
Medium	9.3 ± 2.2	7.4 ± 1.6	5.8 ± 1.4	−38.3 ± 5.2[b]	−20.5 ± 4.3[b]	−22.3 ± 7.1[b]
Large	12.4 ± 2.1	9.8 ± 1.5	6.8 ± 1.4	−44.8 ± 7.2[b]	−20.6 ± 4.3[b]	−30.5 ± 8.2[b]
$CTDI_{vol}$-normalized breast dose coefficients						
Breast Size	ATCM Dose per $CTDI_{vol}$	OTCM Dose per $CTDI_{vol}$	$OTCM_{BP}$ Dose per $CTDI_{vol}$	$OTCM_{BP}$ to ATCM difference (%)	OTCM to ATCM difference (%)	$OTCM_{BP}$ to OTCM difference (%)
Small	1.1 ± 0.1	0.9 ± 0.1	0.7 ± 0.1	−31.4 ± 6.5[b]	−16.9 ± 4.1[b]	−17.3 ± 7.8[b]
Medium	1.0 ± 0.1	0.8 ± 0.1	0.6 ± 0.1	−36.8 ± 5.0[b]	−20.5 ± 4.3[b]	−20.4 ± 6.2[b]
Large	1.0 ± 0.1	0.8 ± 0.1	0.6 ± 0.1	−41.3 ± 5.3[b]	−20.6 ± 4.3[b]	−26.2 ± 4.9[b]

[a]Negative means dose reduction.
[b]represents statistical significant.

4. DISCUSSION

Organ-based tube current modulation techniques have been devised to minimize unnecessary radiation exposure to major radiosensitive organs while maintaining the required image quality. In this work, we evaluated the dose saving potential of an additional breast-positioning technique for organ-based tube current modulation examinations (OTCM). Compared to standard tube current modulation, OTCM offered an average of 19.3 ± 4.5% reduction in breast dose. The breast positioning extended that reduction by an additive 23.8 ± 9.4%. Targeted breast positioning takes a fuller advantage of OTCM for reducing breast dose in body CT examinations.

In this study, a constant $CTDI_{vol}$ value was used for ATCM and OTCM scheme for each phantom. A previous study has argued that OTCM is less dose-economical compared to ATCM, and resulted in a 5–10% $CTDI_{vol}$ increase to maintain image quality.[14] When OTCM is utilized, the x-y modulation is shut off, the Z-plane mA is generated based on

TABLE IV. Fitting coefficients of breast dose and $CTDI_{vol}$-normalized breast dose coefficients fitted vs. breast mass.

	Breast dose			$CTDI_{vol}$-normalized breast dose coefficients		
	$p_{D,1}(kg^{-1})$	$p_{D,2}$	*RMSE*	$p_{h,1}(kg^{-1})$	$p_{h,2}$	*RMSE*
ATCM	2.7	6.58	2.18	−0.007	1.042	0.073
OTCM	1.99	5.45	1.57	−0.027	0.87	0.098
$OTCM_{BP}$	0.94	4.83	1.57	−0.063	0.735	0.084

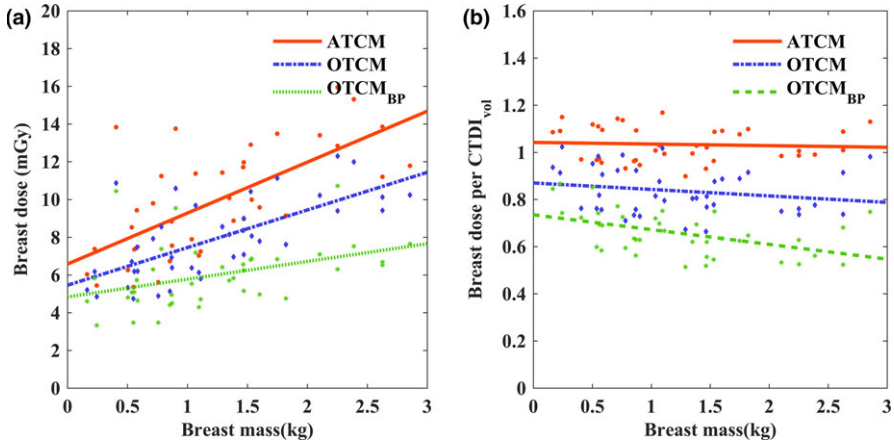

FIG. 8. (a) breast dose and (b) $CTDI_{vol}$-normalized breast dose coefficients linearly fitted to breast mass scanned with ATCM, OTCM, and $OTCM_{BP}$ as Eq (2). [Color figure can be viewed at wileyonlinelibrary.com]

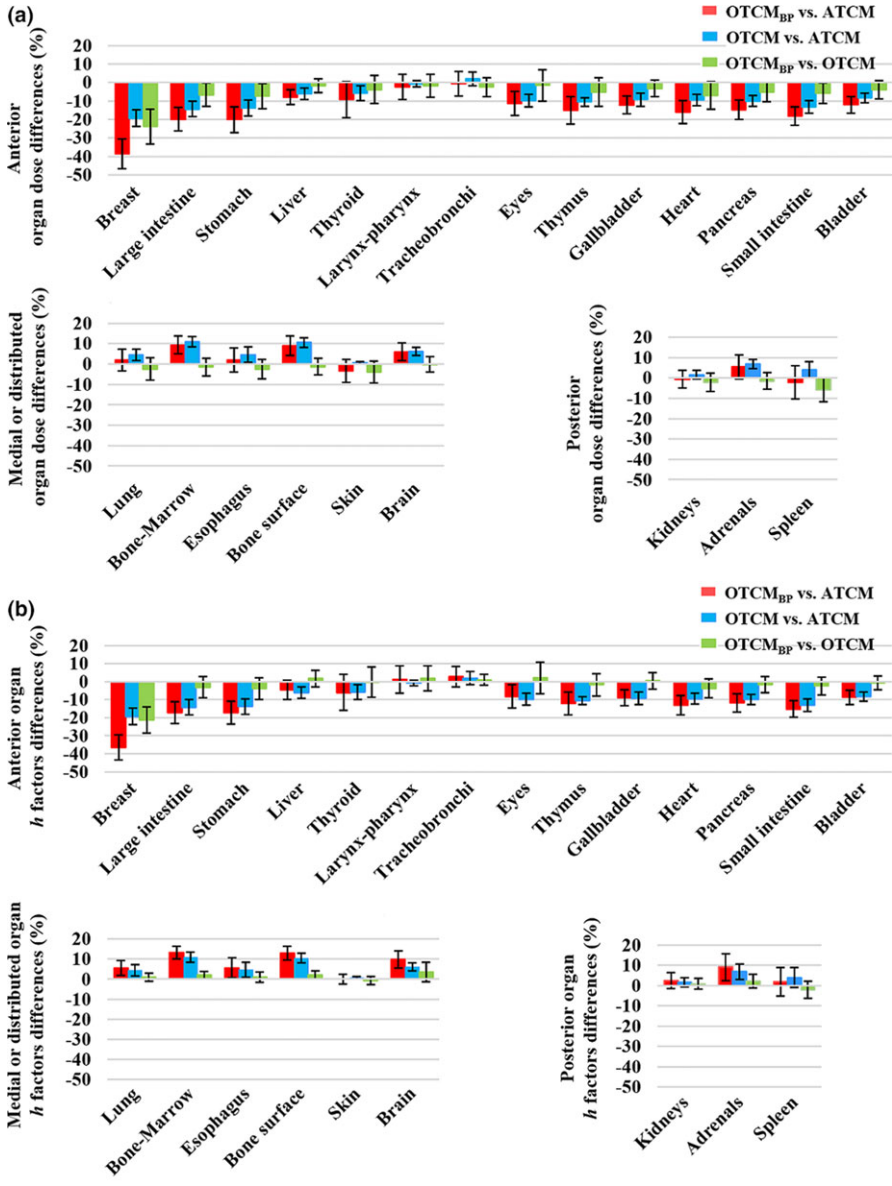

FIG. 9. Differences in (a) organ dose and (b) $CTDI_{vol}$-normalized organ dose coefficients across ATCM, OTCM, and $OTCM_{BP}$. [Color figure can be viewed at wileyonlinelibrary.com]

TABLE V. Average effective dose and the difference between ATCM, OTCM, and $OTCM_{BP}$.[a]

Effective dose (ED)						
Breast Size	ATCM ED (mSv)	OTCM ED (mSv)	$OTCM_{BP}$ ED (mSv)	$OTCM_{BP}$ to ATCM difference (%)	OTCM to ATCM difference (%)	$OTCM_{BP}$ to OTCM difference (%)
Small	4.2 ± 1.1	3.9 ± 0.97	3.7 ± 1.0	−11.2 ± 3.0[b]	−5.6 ± 1.7[b]	−5.9 ± 4.1[b]
Medium	4.7 ± 0.88	4.5 ± 0.81	4.2 ± 0.87	−12.4 ± 3.6[b]	−5.8 ± 1.9[b]	−7.0 ± 4.2[b]
Large	5.6 ± 0.77	5.3 ± 0.71	4.8 ± 0.78	−15.2 ± 6.0[b]	−5.5 ± 1.4[b]	−10.3 ± 6.4[b]
All models	4.8 ± 1.1	4.6 ± 1.0	4.2 ± 1.0	−12.9 ± 4.6[b]	−5.6 ± 1.7[b]	−7.7 ± 5.2[b]
ED normalized by dose-length-product (DLP)						
Breast Size	ATCM ED/DLP (mSv/mGy-cm)	OTCM ED/DLP (mSv/mGy-cm)	$OTCM_{BP}$ ED/DLP (mSv/mGy-cm)	$OTCM_{BP}$ to ATCM difference (%)	OTCM to ATCM difference (%)	$OTCM_{BP}$ to OTCM difference (%)
Small	0.022 ± 0.002	0.021 ± 0.002	0.020 ± 0.001	−9.8 ± 2.0[b]	−5.6 ± 1.7[b]	−4.4 ± 2.6[b]
Medium	0.021 ± 0.002	0.020 ± 0.002	0.019 ± 0.002	−10.3 ± 3.8[b]	−5.8 ± 1.9[b]	−4.8 ± 3.3[b]
Large	0.020 ± 0.002	0.019 ± 0.002	0.018 ± 0.002	−9.7 ± 2.3[b]	−5.5 ± 1.4[b]	−4.5 ± 1.6[b]
All models	0.021 ± 0.002	0.020 ± 0.002	0.019 ± 0.002	−9.9 ± 2.7[b]	−5.6 ± 1.7[b]	−4.6 ± 2.5[b]

[a]Negative means dose reduction.
[b]represents statistical significant change.

the average of AP and LAT attenuation. If techniques permit, keeping x-y plane modulation in OTCM would be more dose efficient. We simulated this scenario ($OTCM_{ideal}$), reducing mA_{ATCM} by 80% and a corresponding increase in the remaining projections. The dose reduction was larger in anterior organs. The dose for heart and thymus was reduced by 14.7 ± 3.4% and 20.0 ± 4.6%, respectively. The dose increase was smaller in distributed and posterior organs (except for spleen). No significant change was noted in lung, esophagus, and kidneys.

To take full advantage of OTCM, breast-positioning techniques have been studied to constrain the breast to within the dose reduction zone. Seidenfuss et al. have demonstrated that a normal brassiere can constrain more breast tissue within the dose reduction zone.[44] However, in that implementation, the breasts are still not fully sheltered, especially in women with larger breasts where only 83.3% of the volume is constrained. Additionally, the study did not evaluate the breast dose. In this study, we simulated the breast-positioning technique that can optimize breast position beyond a normal brassiere's support by compressing more breast tissue to within the dose reduction zone. To ensure the modeled breast locations reflect real scenario, the percentage of breast tissue within the dose reduction zone was compared with those reported in literature. Seidenfuss et al. reported breast volumes within dose reduction zone on CT images from 578 female patients with and without brassiere.[44] On average, 60.4 ± 24.7% and 91.3 ± 9.4% of breast volume was within dose reduction zone without and with a brassiere, respectively.[44] In our work, the average breast tissue within the dose reduction zone was 64.6 ± 15.2% originally, and increased to 93.8 ± 4.0% after applying BP. The ratio of breast within the dose reduction zone is higher in this study compared to Seidenfuss et al. because the breast tissue was compressed closer toward the center of the torso. To implement the studied breast-positioning technique clinically, we recommend the use of sports brassiere with foam padding.

The breast dose savings of OTCM and $OTCM_{BP}$ from ATCM were compared with physical phantoms reported by literature. Comparing OTCM to ATCM reduction for an anthropomorphic phantom with breast attachment, Lungren *et al.* reported the anterior and posterior breast dose reduction of 29–45% and 9–19%, respectively.[16] Our results were generally consistent; from ATCM to OTCM, the average breast dose reduction ranges at 11.0–28.7%. For ATCM to $OTCM_{BP}$, the breast dose reduction ranges at 21.0–51.8% and when normalized by $CTDI_{vol}$, the corresponding reduction ranges at 20.6%–48.1%. Another study reported that breast dose was reduced by 34%, 34%, and 39% with OTCM compared to ATCM for small, medium, and large semi-anthropomorphic phantoms (30 × 20, 35 × 25, 4 × 30 cm in lateral and posterior–anterior dimension).[14] To derive breast dose corresponding to the above average chest diameter in our study, the breast dose was fitted to chest diameter as an exponential function [Eq. (4)] (Fig. 11). On average, compared to ATCM, OTCM reduced breast dose by 13.1%, 18.1%, and 22.8%, and *h* factors by 12.7%, 18.0%, and 23.0%. The OTCM savings in our study was smaller compared to the literature, as the XCAT breasts were explicitly modeled, while the phantoms used in other studies were with "underdeveloped" breasts (i.e., the breasts were not spread).[6,13,14,16,45] Thus, more lateral portions of the XCAT breasts were in the dose-increased zone. The full advantage of OTCM was not taken without BP. The $OTCM_{BP}$ saved the breast dose by 34.4%, 38.1%, 41.5% and *h* factors by 30.1%, 35.3%, and 40.2% for phantoms with 25 cm, 30 cm, and 35 cm chest diameters, respectively.

Using the same $CTDI_{vol}$, OTCM reduced the effective dose, this can be explained by the fact that most of the radiosensitive organs are located anteriorly.[46] Lungren et al. reported the effective dose by evaluating the organ dose recorded by dosimeters for an anthropomorphic physical phantom. The results were 4.41 ± 0.3 mSv (after scanning $CTDI_{vol}$ 6.94 mGy) and 5.25 ± 0.36 mSv (after scanning $CTDI_{vol}$ 7.51 mGy) for ATCM and OTCM, respectively.[16]

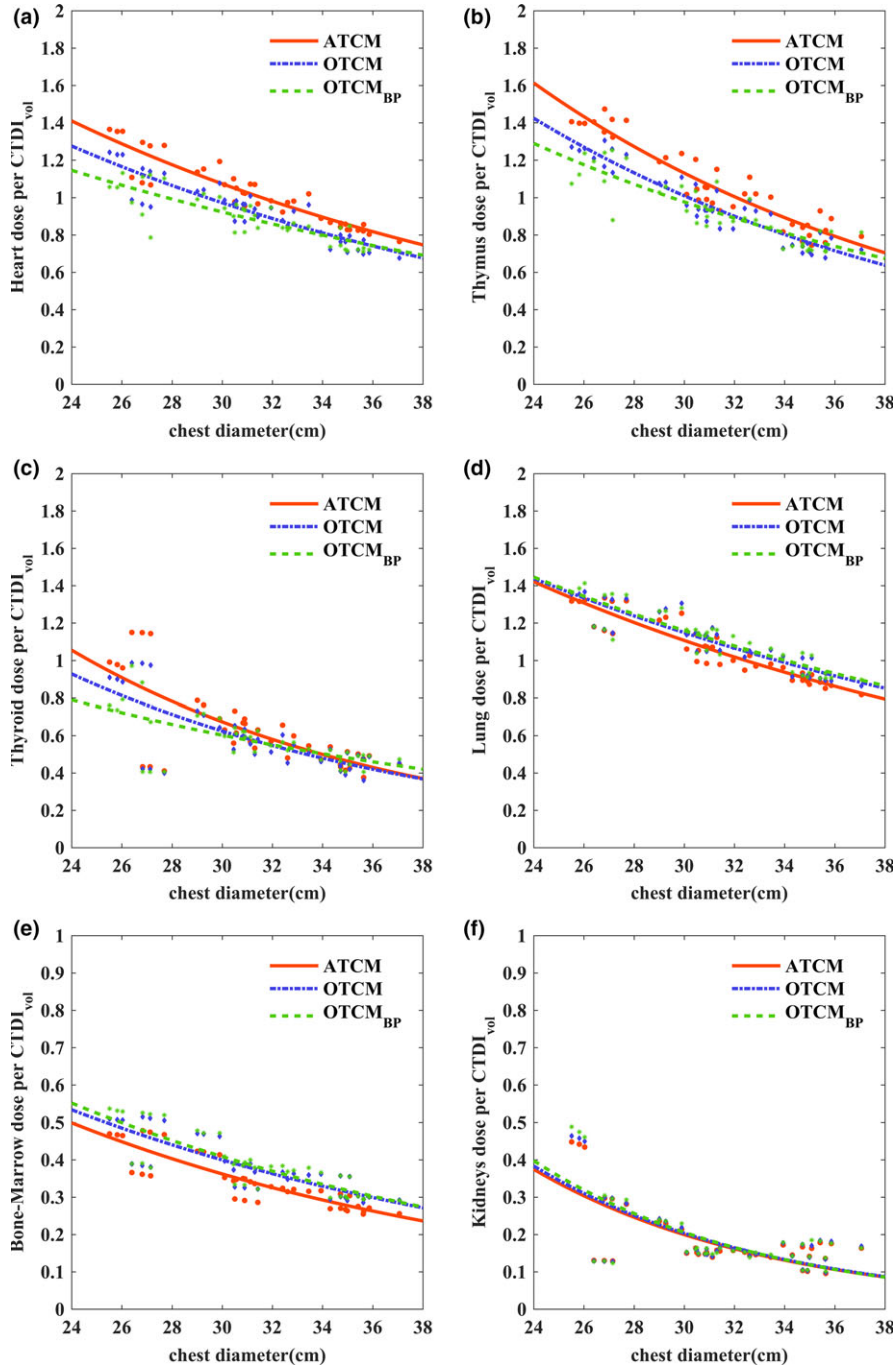

FIG. 10. The CTDI$_{vol}$-normalized organ dose coefficients fitted against phantom chest diameters as shown in Eq (4). Example organs from (a–c) anterior, (d,e) medial or distributed, and (f) posterior groups. [Color figure can be viewed at wileyonlinelibrary.com]

The discrepancy between Lungren et al. and this study can be explained by the fact that the CTDI$_{vol}$ used in this study was constant between OTCM and ATCM, while the CTDI$_{vol}$ for OTCM is generally 5–10% higher as noted previously.

Other organ doses were also compared with physical phantoms. Lungren et al. has reported anterior organ dose reduced 17–47%; posterior organ dose significantly increased; lateral and inner organ dose showed similar results.[16] Our results were consistent on some typical anterior and posterior organs. Thymus and kidney dose changed by 10.5% and −1.6% (7% and −1% from Lungren et al.). The skin dose profile was also compared with measurement of physical phantoms from the literature. The skin dose was sampled and interpolated within 360 degrees for each phantom on one selected slice that contains large volume of breast tissue. The interpolated skin dose was further averaged across all phantoms. Duan et al. reported surface dose of anthropomorphic phantoms receiving OTCM and fixed mA scan (mA$_{fix}$).[13] To compare our results to those of Duan et al., the skin dose was normalized by CTDI$_{vol}$ and scaled to unit

TABLE VI. Fitting parameters of $CTDI_{vol}$-normalized organ dose coefficients (h factors) with respect to chest diameter [Eq. (4)].

	ATCM			OTCM			$OTCM_{BP}$		
Organ	$\alpha_{h,ATCM}$	$\beta_{h,ATCM}$	R^2	$\alpha_{h,OTCM}$	$\beta_{h,OTCM}$	R^2	$\alpha_{h,OTCM,BP}$	$\beta_{h,OTCM,BP}$	R^2
Anterior organs									
Breast	−0.01	0.47	0.45	−0.03	0.65	0.56	−0.03	0.51	0.47
Large intestine	0.04	−3.43	0.12	0.03	−3.44	0.10	0.04	−3.71	0.15
Stomach	−0.05	1.05	0.31	−0.05	0.96	0.30	−0.04	0.44	0.20
Liver	−0.03	0.36	0.46	−0.03	0.25	0.38	−0.02	0.12	0.28
Thyroid	−0.08	1.85	0.53	−0.07	1.51	0.53	−0.05	0.85	0.41
Larynx–pharynx	−0.01	−1.09	0.09	−0.01	−1.18	0.06	0.00	−1.51	0.00
Trach-bronchi	−0.06	1.89	0.94	−0.05	1.65	0.92	−0.05	1.53	0.86
Eyes	0.01	−4.55	0.09	0.00	−4.39	0.01	0.02	−4.82	0.16
Thymus	−0.06	1.90	0.89	−0.06	1.73	0.89	−0.05	1.37	0.75
Gallbladder	0.01	−2.17	0.02	0.01	−2.16	0.01	0.01	−2.26	0.02
Heart	−0.05	1.43	0.86	−0.05	1.33	0.82	−0.04	1.00	0.71
Pancreas	−0.03	−0.32	0.09	−0.03	−0.45	0.09	−0.02	−0.78	0.04
Small intestine	0.03	−3.26	0.08	0.03	−3.24	0.06	0.03	−3.51	0.11
Bladder	−0.01	−5.76	0.02	−0.01	−5.83	0.02	−0.01	−5.88	0.01
Medial or distributed organs									
Lung	−0.04	1.35	0.87	−0.04	1.26	0.84	−0.04	1.25	0.81
Bone marrow	−0.05	0.59	0.77	−0.05	0.53	0.72	−0.05	0.61	0.71
Esophagus	−0.06	1.69	0.94	−0.05	1.46	0.88	−0.05	1.41	0.84
Bone surface	−0.05	0.88	0.81	−0.04	0.83	0.77	−0.04	0.88	0.76
Skin	−0.04	−0.47	0.63	−0.04	−0.46	0.65	−0.04	−0.39	0.70
Brain	−0.01	−4.13	0.06	−0.01	−4.11	0.04	−0.01	−4.18	0.03
Posterior organs									
Kidneys	−0.11	1.54	0.48	−0.11	1.58	0.46	−0.11	1.71	0.46
Adrenals	−0.10	2.21	0.55	−0.10	2.48	0.54	−0.11	2.78	0.54
Spleen	−0.05	0.99	0.40	−0.04	0.83	0.29	−0.03	0.64	0.22

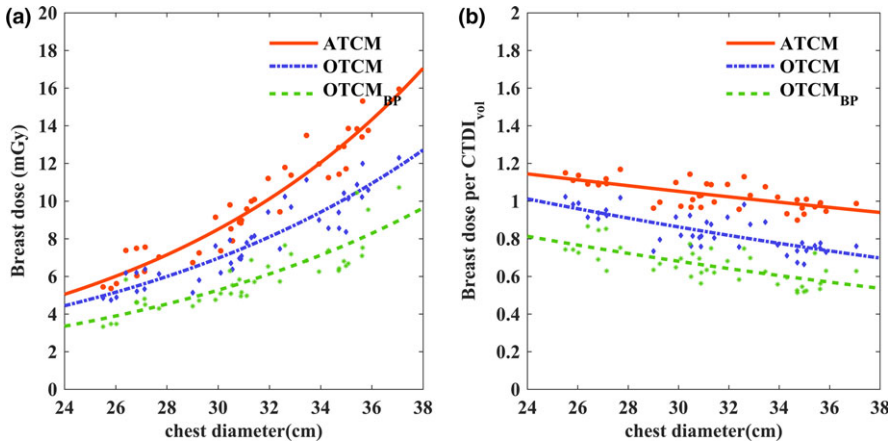

FIG. 11. (a) Breast dose and (b) $CTDI_{vol}$-normalized breast dose from ATCM, OTCM, and $OTCM_{BP}$ simulations fitted to chest diameter as Eq (4). [Color figure can be viewed at wileyonlinelibrary.com]

average. Our results showed excellent agreement with the measurement from physical phantoms (Fig. 12). For OTCM, the dose was unsymmetrical on the left and right reduction zone, which was due to unequal upward- and downward-transition times. Compared to mA_{fix}, the mA_{ATCM} is generally larger in LAT and smaller in AP.

Although the use of a patient's own brassiere is cost efficient, a specially designed BP support would be superior as it compresses more of the breast tissue within the dose reduction zone, especially the outer quadrant of the breast, which more than half of breast carcinoma first occurs.[18,19,47] With a normal brassiere, 17% of the breast is outside the dose

reduction zone for large-sized breasts.[44] With the implemented BP, the portion of breast tissue within the dose-increased zone decreases to 6%. Furthermore, BP constrains an average constant portion (94%) of breast tissue within the dose reduction zone in all groups. However, normal brassiere's performance varies among different breast-size groups.[44] The dose savings effect and potential artifacts in CT images with various normal brassieres is yet to be examined. A standardized BP allows one to accurately monitor dose and prospectively optimize CT procedure.

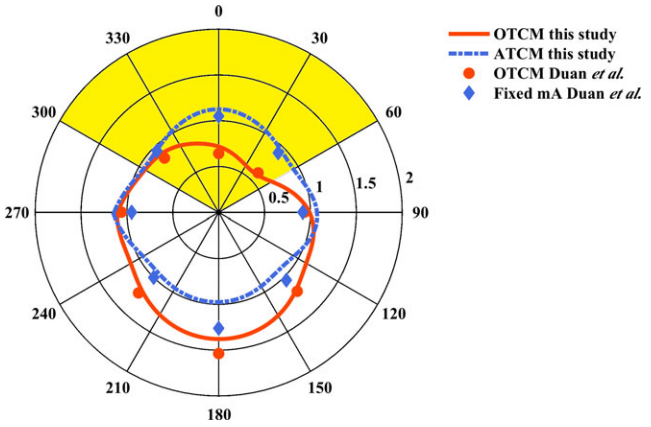

FIG. 12. Skin dose simulated with computerized phantom with ATCM and OTCM from this study compared skin dose measured with physical phantoms with OTCM and fixed mA from Duan *et al.* The dose was averaged to a unit mean for comparisons. For this study, the skin dose profile was averaged across all phantoms. The dose reduction zone is shaded. [Color figure can be viewed at wileyonlinelibrary.com]

For all the organs within the scan coverage, lungs have the same radiosensitivity as breasts.[41] Our results showed that lung dose only increased slightly using OTCM, compared to ATCM. As the tube current was decreased anteriorly and increased posteriorly, the lung dose is non-uniformly distributed. To estimate the distribution of lung dose, lung dose was estimated at five different lung ROIs on the dose distribution plot located as shown in Fig. 13. The lung dose was averaged over each ROI across 39 phantoms for each modulation scheme. The results showed that anterior lung regions and posterior lung regions have lower and higher dose, respectively, for OTCM, compared to ATCM. For lung regions in the central line of AP direction, the lung doses are similar for OTCM and ATCM. Lungren et al. reported that the lung dose decreased by 7% (average of 12% and 2%) and 13% (average of 18% and 7%) for anterior and posterior lung regions, respectively.[16] In their study, the decrease of lung dose in posterior regions may be a result of sampling posterior lung dose more centrally compared to our sampling scheme.

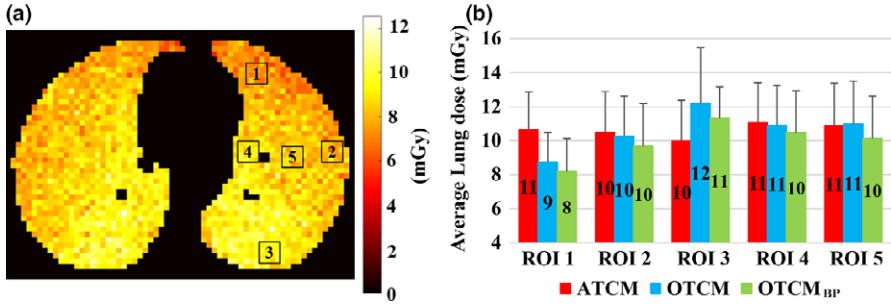

FIG. 13. (a) Example of five ROIs drawn on dose distribution plots to evaluate the non-uniform distribution of lung dose. (b) For each ROI, the average dose value was calculated. [Color figure can be viewed at wileyonlinelibrary.com]

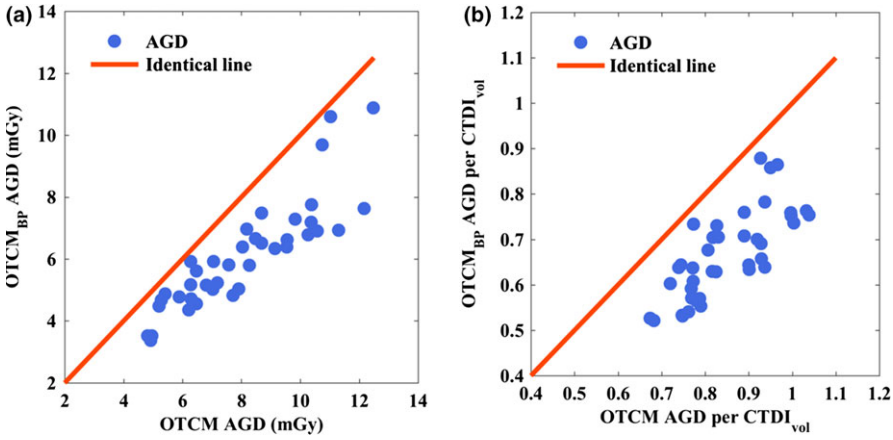

FIG. 14. (a) average glandular dose (AGD) and (b) $CTDI_{vol}$-normalized-AGD simulated by $OTCM_{BP}$ vs. OTCM. The AGD was derived by Eq. (5). [Color figure can be viewed at wileyonlinelibrary.com]

In this study, the primary focus was breast dose. However, the most relevant component of breast dose is average glandular dose (AGD). A side study was conducted to ascertain how the two are related. A prior study has derived the AGD from homogeneous breast tissue via simulation.[48] For each photon–material interaction, the dose to breast tissue was corrected to the glandular tissue by the ratio of glandular to breast mass attenuation coefficients at that energy level.[48] Using this approach, a conversion was derived as

$$r_{breast-to-AGD} = \sum \frac{\frac{\mu}{\rho}(E_i, glandular)}{\frac{\mu}{\rho}(E_i, breast)} P(E_i), \quad (5)$$

where $P(E_i)$ is source energy spectrum, filtered by the bowtie filter, and $\frac{\mu}{\rho}(E_i, glandular)$ and $\frac{\mu}{\rho}(E_i, breast)$ are the mass attenuation coefficients for glandular and breast tissues at energy E_i, respectively. Assuming the spectrum's further filtering by patient body can be ignored, $r_{breast-to-AGD}$ was computed to be 1.015 and 1.031 for the 50/50 breast and 20/80 breast, respectively. This indicates the breast dose and ADG are closely correlated at CT energies. Figure 14 shows a plot of average glandular dose for $OTCM_{BP}$ vs. OTCM. Please note, homogeneous distribution of glandular dose is an approximation. Future study is warranted to simulate heterogeneous breast tissue.

This work has several limitations. First, the dose coefficient estimation was limited to one CT scanner. Second, although the dose reduction potential was demonstrated, an optimized positioning technique with minimum dose and patient comfort is yet to be defined. For each phantom, only one breast positioning was simulated. Third, image quality was not examined in this study. In previous studies, no significant difference in noise and CT numbers have been reported when comparing OTCM with ATCM or fixed mA scans using physical phantoms.[13,14,16] Neither were streaking and beam hardening artifacts with perceivable differences found. In the work by Seidenfuss et al., the image quality was assessed for women scanned with OTCM, with and without a normal brassiere; no artifacts were reported.[44] A similar study will be conducted for $OTCM_{BP}$ in the future. Fourth, the mA profile was generated theoretically, as the actual mA in a CT system may not be predicted merely by patient attenuation.[24] For example, the mA profile may overshoot at the beginning of a scan.[49] To ensure the tube current profile in general agrees with the physical behavior, the skin dose was sampled and compared to studies measuring skin dose on physical phantoms and our results showed strong agreement (Fig. 12). Future studies may include modeling the mA profile taking into account actual physical behaviors. Fifth, the *h* factors and the comparisons for different modulation schemes reported in this study was specific to the mA scheme (average modulation strength). The study of other modulation strengths as well as other organ-based tube current modulation schemes used by various scanners and the associated effect on organ doses would be of value. However, as $CTDI_{vol}$ is a strong normalizing and a major factor significantly influencing organ dose, the $CTDI_{vol}$-normalized organ dose dataset can reasonably characterize the net effect of modulation or breast positioning.

5. CONCLUSION

In this study, the dose reduction potential of alternate breast positioning was evaluated for organ-based TCM examinations. Keeping $CTDI_{vol}$ constant, on average, compared to ATCM, OTCM reduced the breast dose by ~20%. The average breast dose was further decreased by an additional 23% with targeted breast positioning. Targeted breast positioning is needed to take full advantage of OTCM for reducing breast dose in body CT examinations.

ACKNOWLEDGMENT

The authors thank Juan Carlos Ramirez-Giraldo for valuable discussions about the organ-based tube current modulation technique.

CONFLICTS OF INTEREST

E.S. has grant support unrelated to this study from Siemens Medical Solutions and GE Healthcare. Other authors have no relevant conflicts of interest to disclose.

[a]Author to whom correspondence should be addressed. Electronic mail: samei@duke.edu

REFERENCES

1. IMV. CT Market Outlook Report. 2014.
2. Evens RG, Mettler F. National CT use and radiation exposure: United States 1983. *Am J Roentgenol*. 1985;144:1077–1081.
3. Brenner DJ, Hall EJ. Computed tomography – an increasing source of radiation exposure. *N Engl J Med*. 2007;357:2277–2284.
4. McCollough CH, Chen GH, Kalender W, et al. Achieving routine submillisievert CT scanning: report from the summit on management of radiation dose in CT. *Radiology*. 2012;264:567–580.
5. Vollmar SV, Kalender WA. Reduction of dose to the female breast in thoracic CT: a comparison of standard-protocol, bismuth-shielded, partial and tube-current-modulated CT examinations. *Eur Radiol*. 2008;18:1674–1682.
6. Wang J, Duan X, Christner JA, Leng S, Grant KL, McCollough CH. Bismuth shielding, organ-based tube current modulation, and global reduction of tube current for dose reduction to the eye at head CT. *Radiology*. 2012;262:191–198.
7. Valentin J. *The 2007 recommendations of the international commission on radiological protection*. Oxford: Elsevier; 2007.
8. Angel E, Yaghmai N, Jude CM, et al. Dose to radiosensitive organs during routine chest CT: effects of tube current modulation. *Am J Roentgenol*. 2009;193:1340.
9. Fricke BL, Donnelly LF, Frush DP, et al. In-plane bismuth breast shields for pediatric CT: effects on radiation dose and image quality using experimental and clinical data. *Am J Roentgenol*. 2003;180:407–411.
10. McLaughlin D, Mooney R. Dose reduction to radiosensitive tissues in CT. Do commercially available shields meet the users' needs? *Clin Radiol*. 2004;59:446–450.
11. Kubo T, Lin P-JP, Stiller W, et al. Radiation dose reduction in chest CT: a review. *Am J Roentgenol*. 2008;190:335–343.
12. Raissaki M, Perisinakis K, Damilakis J, Gourtsoyiannis N. Eye-lens bismuth shielding in paediatric head CT: artefact evaluation and reduction. *Pediatr Radiol*. 2010;40:1748–1754.

13. Duan X, Wang J, Christner JA, Leng S, Grant KL, McCollough CH. Dose reduction to anterior surfaces with organ-based tube-current modulation: evaluation of performance in a phantom study. *Am J Roentgenol*. 2011;197:689–695.
14. Wang J, Duan X, Christner JA, Leng S, Yu L, McCollough CH. Radiation dose reduction to the breast in thoracic CT: comparison of bismuth shielding, organ-based tube current modulation, and use of a globally decreased tube current. *Med Phys*. 2011;38:6084–6092.
15. Samei E. Pros and cons of organ shielding for CT imaging. *Pediatr Radiol*. 2014;44:495–500.
16. Lungren MP, Yoshizumi TT, Brady SM, et al. Radiation dose estimations to the thorax using organ-based dose modulation. *Am J Roentgenol*. 2012;199:W65–W73.
17. Taylor S, Litmanovich DE, Shahrzad M, Bankier AA, Gevenois PA, Tack D. Organ-based tube current modulation: are women's breasts positioned in the reduced-dose zone? *Radiology*. 2014;274:260–266.
18. Lee AHS. Why is carcinoma of the breast more frequent in the upper outer quadrant? a case series based on needle core biopsy diagnoses. *The Breast*. 2005;14:2.
19. Fortner KB, Szymanski LM, Fox HE, Wallach EE. *The Johns Hopkins manual of gynecology and obstetrics*. Philadelphia, PA: Lippincott Williams & Wilkins; 2007.
20. Segars WP, Bond J, Frush J, et al. Population of anatomically variable 4D XCAT adult phantoms for imaging research and optimization. *Med Phys*. 2013;40:043701.
21. Segars W, Mahesh M, Beck T, Frey E, Tsui B. Realistic CT simulation using the 4D XCAT phantom. *Med Phys*. 2008;35:3800–3808.
22. Segars W, Sturgeon G, Mendonca S, Grimes J, Tsui BM. 4D XCAT phantom for multimodality imaging research. *Med Phys*. 2010;37:4902–4915.
23. Valentin J. Basic anatomical and physiological data for use in radiological protection: reference values: ICRP Publication 89. *Annals of the ICRP*. 2002;32:1–277.
24. Li X, Segars WP, Samei E. The impact on CT dose of the variability in tube current modulation technology: a theoretical investigation. *Phys Med Biol*. 2014;59:4525.
25. Yaffe M, Boone J, Packard N, et al. The myth of the 50-50 breast. *Med Phys*. 2009;36:5437–5443.
26. Richard Hammerstein G, Miller DW, White DR, Ellen Masterson M, Woodard HQ, Laughlin JS. Absorbed radiation dose in mammography 1. *Radiology*. 1979;130:485–491.
27. Li X, Samei E, Segars WP, et al. Patient-specific radiation dose and cancer risk estimation in CT: part I. Development and validation of a Monte Carlo program. *Med Phys*. 2011;38:397–407.
28. Schnabel JA, Tanner C, Castellano-Smith AD, et al. Validation of nonrigid image registration using finite-element methods: application to breast MR images. *IEEE Trans Med Imaging*. 2003;22:238–247.
29. Tanner C, Degenhard A, Schnabel J, et al. A method for the comparison of biomechanical breast models. In *Proceedings IEEE Workshop on Mathematical Methods in Biomedical Image Analysis (MMBIA 2001)*.
30. Kellner AL, Nelson TR, Cerviño LI, Boone JM. Simulation of mechanical compression of breast tissue. *IEEE Trans Biomed Eng*. 2007;54:1885–1891.
31. Hsu CM, Palmeri ML, Segars WP, Veress AI, Dobbins JT III. An analysis of the mechanical parameters used for finite element compression of a high-resolution 3D breast phantom. *Med Phys*. 2011;38:5756–5770.
32. Maas SA, Ellis BJ, Ateshian GA, Weiss JA. FEBio: finite elements for biomechanics. *J Biomech Eng*. 2012;134:011005.
33. Li X, Samei E, Segars WP, et al. Patient-specific radiation dose and cancer risk estimation in CT: part II. Application to patients. *Med Phys*. 2011;38:408–419.
34. Baro J, Sempau J, Fernández-Varea J, Salvat F. PENELOPE: an algorithm for Monte Carlo simulation of the penetration and energy loss of electrons and positrons in matter. *Nucl Instrum Methods Phys Res, Sect B*. 1995;100:31–46.
35. Sempau J, Fernandez-Varea J, Acosta E, Salvat F. Experimental benchmarks of the Monte Carlo code PENELOPE. *Nucl Instrum Methods Phys Res, Sect B*. 2003;207:107–123.
36. Tian X, Li X, Segars WP, Paulson EK, Frush DP, Samei E. Pediatric chest and Abdominopelvic CT: organ dose estimation based on 42 patient models. *Radiology*. 2014;270:535–547.
37. Li X, Samei E, Segars WP, Sturgeon GM, Colsher JG, Frush DP. Patient-specific radiation dose and cancer risk for pediatric chest CT. *Radiology*. 2011;259:862–874.
38. Tian X, Li X, Segars WP, Frush DP, Samei E. Prospective estimation of organ dose in CT under tube current modulation. *Med Phys*. 2015;42:1575–1585.
39. AAPM. Use of water equivalent diameter for calculating patient size and size-specific dose estimates (SSDE) in CT, AAPM Report No. 220. American Association of Physicists in Medicine, College Park, MD, 2014.
40. AAPM. Size-specific dose estimates (SSDE) in pediatric and adult body CT examinations, AAPM Report No. 204. American Association of Physicists in Medicine, College Park, MD, 2011.
41. Protection R. ICRP publication 103. *Ann. ICRP*. 2007;37:2.
42. Sahbaee P, Segars WP, Samei E. Patient-based estimation of organ dose for a population of 58 adult patients across 13 protocol categories. *Med Phys*. 2014;41:072104.
43. Turner AC, Zhang D, Khatonabadi M, et al. The feasibility of patient size-corrected, scanner-independent organ dose estimates for abdominal CT exams. *Med Phys*. 2011;38:820–829.
44. Seidenfuss A, Mayr A, Schmid M, Uder M, Lell MM. Dose reduction of the female breast in chest CT. *Am J Roentgenol*. 2014;202:W447–W452.
45. O'Hea BJ, Hill AD, El-Shirbiny AM, et al. Sentinel lymph node biopsy in breast cancer: initial experience at Memorial Sloan-Kettering Cancer Center. *J Am Coll Surg*. 1998;186:423–427.
46. Dixon MT, Loader RJ, Stevens GC, Rowles NP. An evaluation of organ dose modulation on a GE optima CT660-computed tomography scanner. *J Appl Clin Med Phys* 2016;17:380–391.
47. Darbre PD. Recorded quadrant incidence of female breast cancer in Great Britain suggests a disproportionate increase in the upper outer quadrant of the breast. *Anticancer Res*. 2005;25:2543–2550.
48. Boone JM, Nelson TR, Lindfors KK, Seibert JA. Dedicated breast CT: radiation dose and image quality evaluation 1. *Radiology*. 2001;221:657–667.
49. Khatonabadi M, Kim HJ, Lu P, et al. The feasibility of a regional CTDIvol to estimate organ dose from tube current modulated CT exams. *Med Phys*. 2013;40:051903.